Available online at www.sciencedirect.com
SCIENCE DIRECT®
Journal of Computational Physics 208 (2005) 435–454
JOURNAL OF COMPUTATIONAL PHYSICS
www.elsevier.com/locate/jcp

An asymptotically stable compact upwind-biased finite-difference scheme for hyperbolic systems

A. Jocksch [a,*], N.A. Adams [b], L. Kleiser [a]

[a] Institute of Fluid Dynamics, ETH Zürich, CH-8092 Zürich, Switzerland
[b] Institute of Aerodynamics, Technische Universität München, D-85747 Garching, Germany

Received 26 July 2004; received in revised form 31 January 2005; accepted 31 January 2005
Available online 26 April 2005

Abstract

Asymptotic stability of high-order finite-difference schemes for linear hyperbolic systems is investigated using the Nyquist criterion of linear-system theory. This criterion leads to a sufficient stability condition which is evaluated numerically. A fifth-order compact upwind-biased finite-difference scheme is developed which is asymptotically stable, according to the Nyquist criterion, for linear 2×2 systems. Moreover, this scheme is optimised with respect to its dispersion properties. The suitability of the scheme for discretisation of the compressible Navier–Stokes equations is demonstrated by computing inviscid and viscous eigensolutions of compressible Couette flow.

Keywords: Compact finite-difference schemes; Stability

1. Introduction

A major challenge for the application of high-order finite-difference schemes to hyperbolic partial differential equations is to find stable boundary closures while maintaining the global order of accuracy r implied by the interior scheme. For this purpose, the boundary scheme must have a local order of at least $r - 1$ [11]. The Gustafsson–Kreiss–Sundström (GKS) stability theory provides the means for decoupling the analysis of boundary scheme and interior scheme [6]. For long-time integration, however, the more restrictive asymptotic stability is required [6]. Asymptotic stability of a scheme for the scalar case does not guarantee this property for systems of evolution equations, e.g. for 2×2 systems [6,7].

* Corresponding author. Tel.: +49 1 63 25273; fax: +49 1 63 21147.
E-mail address: jocksch@ifd.mavt.ethz.ch (A. Jocksch).

0021-9991/$ - see front matter
doi:10.1016/j.jcp.2005.01.030

One approach to ensure asymptotic stability for systems is the summation-by-parts technique [7] which is based on an energy estimate. However, the summation-by-parts condition requires the difference schemes to obey certain symmetry conditions in combination with a specific boundary treatment.

In this paper, asymptotic stability for systems is addressed employing linear-system theory. We recognise that 2×2 linear hyperbolic systems correspond to feedback-coupled systems of linear-system theory for which a necessary and sufficient stability condition is the Nyquist criterion [8]. If the Nyquist criterion is satisfied stability for 2×2 systems is a consequence of asymptotic stability of the scalar case. For evaluating the Nyquist criterion, the frequency response of semi-discretisations to a harmonic excitation at the inflow boundary is evaluated numerically. A compact upwind-biased finite-difference discretisation is considered, such as suggested in [3,17]. The compactness of the scheme provides a high-order discretisation and high resolution properties on a narrow stencil. The upwinding property implies intrinsic dissipation at high wavenumbers which damps spurious oscillations due to nonlinear effects (e.g. aliasing), which is a desired property e.g. for turbulent flow simulations.

An unavoidable property of finite-difference schemes is that propagating waves may create spurious waves at the boundaries. Discontinuities of the discretisation scheme, i.e. changes of the scheme's coefficients from one grid point to the next, in general lead to reflections which are determined by the dispersion properties of the scheme [20]. Note that the GKS stability theory can also be interpreted in terms of these spurious waves and wave reflections [18,19]. In order to minimise reflections, certain boundary treatments have been proposed, see [9] for a review. Based on the interior discretisation given by the fifth-order upwind-biased scheme CUVB [2], in the present paper we construct boundary schemes which are asymptotically stable for 2×2 linear hyperbolic systems and are optimised with respect to their dispersion properties at the boundaries. To demonstrate that the desired stability properties transfer to the discretisation of the full Navier–Stokes equations, we apply these schemes to the direct numerical simulation of a standing wave and to inviscid and viscous linear-stability eigensolutions of compressible plane Couette flow.

2. Stability of the scalar problem

Initially, we consider asymptotic stability of the scalar initial-boundary-value problem for the linear advection equation which is the necessary condition for stability for systems,

$$\frac{\partial u}{\partial t}+c\frac{\partial u}{\partial x}=0,\quad 0\leqslant x\leqslant 1,\ t\geqslant 0,\ c>0, \tag{1a}$$

$$u(x,0)=f(x),\ 0\leqslant x\leqslant 1, \tag{1b}$$

$$u(0,t)=u_0(t),\ t\geqslant 0. \tag{1c}$$

Following the method of lines [12,21], a spatial finite-difference discretisation results in the ordinary-differential-equation system for the vector of semi-discrete solutions $u_j(t)\approx u(x_j,t)$ along a set of N lines $x=x_j$, $j=1,\ldots,N$,

$$\mathbf{M}_L\frac{\mathrm{d}\mathbf{u}}{\mathrm{d}t}+c\mathbf{M}_R\mathbf{u}=c\mathbf{b}u_0(t), \tag{2}$$

where $\mathbf{u}=\{u_j\}_{j=1}^{N}$ and the matrices $\mathbf{M}_L$, $\mathbf{M}_R$ and vector $\mathbf{b}$ are sparse (see Appendix A, Eq. (A.2)). Since we are interested in the stability properties of the spatial discretisation we consider here the semi-discrete problem only. For time integration any stable scheme can be used.

With the ansatz $\mathbf{u}=\mathbf{u}_{\mathrm{ev}}\mathrm{e}^{\lambda t}$ and the homogeneous boundary condition $u_0(t)=0$ one obtains the generalised eigenvalue problem

$$-\frac{\lambda}{c}\mathbf{M}_L\mathbf{u}_{\mathrm{ev}} = \mathbf{M}_R\mathbf{u}_{\mathrm{ev}}. \tag{3}$$

For asymptotic stability of scheme (2) for the solution of (1) with homogeneous boundary condition the real parts of all eigenvalues λ of Eq. (3) must satisfy $\mathrm{Re}(\lambda) \leqslant 0$, where for $\mathrm{Re}(\lambda) = 0$ the multiplicity of λ is at most one. To ensure stability also for the inhomogeneous case, eigenvalues with zero real part need to be excluded. Another requirement is Lax stability which for a semi-discretisation is equivalent to the solution being bounded in the limit $\Delta x \to 0$ at a fixed time t [6]. In [6] Lax stability for finite-difference approximations was shown by GKS stability analysis. Since Lax stability is not the main focus in this paper, we follow for this purpose a more pragmatic approach and test a necessary condition (bounded real parts of the eigenvalues) along with a convergence study of the solution for spatial refinement at a fixed time.

3. Transfer function

The stability criterion for systems considered here is based on the transfer function of the scalar initial-boundary-value problem. The solution of this problem is a linear combination of the homogeneous solution and a particular solution. The homogeneous solution of Eq. (2) can be expressed as a linear combination of eigensolutions of Eq. (3). A particular solution can be obtained by a Laplace transform in t of Eq. (2) assuming vanishing initial conditions. This leads to a system of linear equations for $\mathbf{g}(s)$,

$$\mathbf{g}(s) = (s\mathbf{M}_L + c\mathbf{M}_R)^{-1}c\mathbf{b}, \tag{4}$$

where

$$\mathbf{g}(s) = \mathscr{L}\{\mathbf{u}(t)\}/\mathscr{L}\{u_0(t)\} \quad \text{and} \quad s = \delta + \mathrm{i}\Omega, \quad \delta, \Omega \in \mathbb{R}. \tag{5}$$

$\mathbf{g}(s)$ is the transfer function in Laplace space of an inhomogeneity $\mathscr{L}\{u_0(t)\}$ which generates a grid function $\mathscr{L}\{\mathbf{u}(t)\}$ as response. In the case of a purely imaginary $s = \mathrm{i}\Omega$, $\mathbf{g}(\mathrm{i}\Omega)$ represents the frequency response. It can be expressed at each grid point x_j as

$$g_j(\mathrm{i}\Omega) = |g_j(\mathrm{i}\Omega)|\mathrm{e}^{\mathrm{i}\varphi_j(\Omega)} \tag{6}$$

with the amplitude response $|g_j(\mathrm{i}\Omega)|$ and the phase response $\varphi_j(\Omega)$. Note that for $s = \lambda$ the matrix $(s\mathbf{M}_L + c\mathbf{M}_R)$ becomes singular which corresponds to poles of the transfer function $\mathbf{g}(s)$.

The stability criterion for systems considered here is governed by the transfer function of the outflow grid point $g_N(s)$ only. For evaluating finite-difference discretisations we also consider amplitude responses for the grid function on the entire domain which at each grid point represent the magnitude of temporal oscillations. These oscillations originate from the inflow boundary and spread downstream. An ideal amplitude response should be unity for all grid points and frequencies. The phase shift which can be quantified by the phase response is not taken into account here.

Fig. 1 shows amplitude responses of grid functions for different finite-difference schemes in terms of frequencies along grid points j. Considered discretisations are the first-order upwind scheme (Fig. 1(a)), the second-order central scheme with first-order upwind discretisation at the outflow boundary (Fig. 1(b)), the compact sixth-order central scheme with a fourth-order three-point stencil at the points adjacent to the boundary and a third-order stencil at the boundary points [14] (Fig. 1(c)) and the sixth-order summation-by-parts scheme of Strand [16,7] (Fig. 1(d)), herein referred to as UPW1, CEN2, PAD6 and SBP6, respectively. Furthermore, the fifth-order compact upwind-biased scheme CUVB [3,2] (Fig. 1(e), for the discretisation matrices see Appendix B, Eq. (B.1)) is investigated. The inflow boundary condition is enforced strongly on the inflow grid point except for the summation-by-parts scheme where the simultaneous approximation term (SAT) [7] is used, which is a penalty formulation. The amplitude responses exhibit

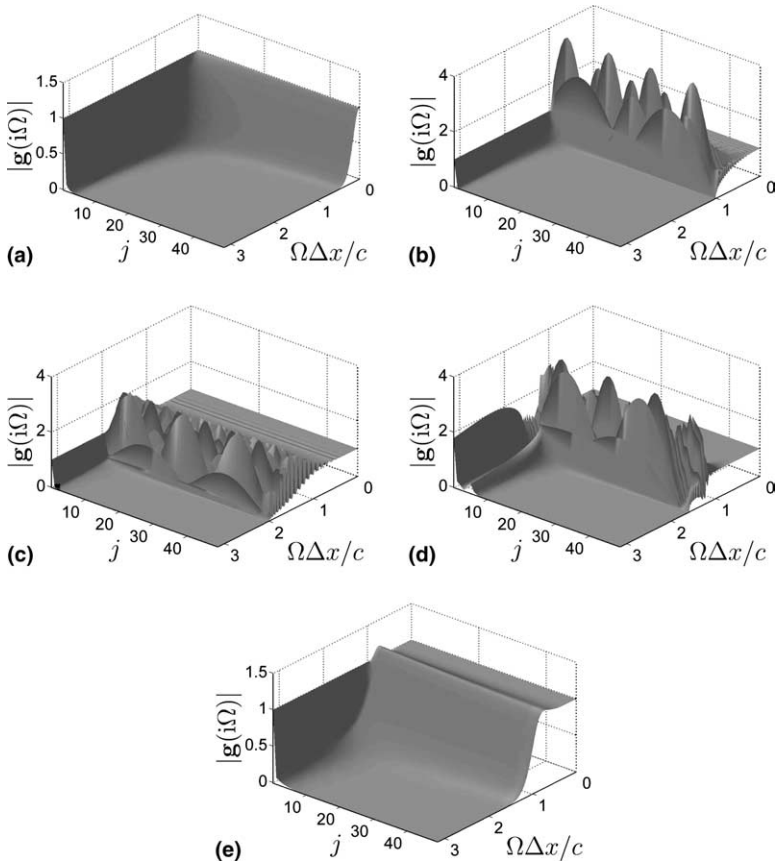

Fig. 1. Amplitude response versus frequency $\Omega\Delta x/c$ along grid points j of schemes (a) first-order upwind (UPW1), (b) second-order central (CEN2), (c) sixth-order compact central (PAD6) [14], (d) sixth-order summation-by-parts of B. Strand with SAT (SBP6) [16,7] and (e) fifth-order compact upwind-biased (CUVB) [3], illustrated for $\Omega\Delta x/c$ in steps of $\pi/500$.

the typical behaviour of coupled oscillator systems. For the central schemes one observes unit amplification for $\Omega = 0$, large amplification peaks close to resonance and a decay to zero for $\Omega \to \infty$ (Figs. 1(b)–(d)). In contrast, the schemes with damping do not show resonance behaviour (Figs. 1(a) and (e)). Except for the SAT boundary condition, the amplitude response at the inflow grid point $j = 0$ is unity. Note that the amplitude response results shown in Fig. 1 are computed for discrete frequencies, which leads to a smeared appearance of the peaks. The desired behaviour of an overall amplitude response of unity is reached approximately at low frequencies where the high-order schemes (PAD6, SBP6 and CUVB) perform better than the low-order discretisations (UPW1, CEN2).

We now focus on the upwind-biased scheme since it has no resonance behaviour. For the interpretation of amplification and resonance in terms of dispersion properties see Section 5.

4. Stability of the system

In general, asymptotic stability for systems can be investigated establishing the eigenvalue problem of the semi-discretisation for the entire system in an analogous fashion to the scalar problem (Eq. (1)–(3)). We apply the Nyquist criterion by which stability for systems can be inferred from investigating the scalar

problem. This is of special interest for the split of the one-dimensional discretisation into several domains, i.e. for a partitioning of the computational domain into subdomains with boundary schemes where on the boundary grid point the outflow boundary value of one domain is imposed as inflow boundary condition to the neighboring domain. As mentioned before, stability of the entire system can be ensured by investigating scalar problems on the individual domains. As model problem, we consider the linear hyperbolic 2×2 system

$$\frac{\partial u}{\partial t}+c\frac{\partial u}{\partial x}=0,\quad \frac{\partial v}{\partial t}-c\frac{\partial v}{\partial x}=0,\qquad 0\leqslant x\leqslant 1,\ t\geqslant 0,\ c>0, \tag{7a}$$

$$u(x,0)=f_u(x),\quad v(x,0)=f_v(x),\qquad 0\leqslant x\leqslant 1, \tag{7b}$$

$$u(0,t)=v(0,t),\quad v(1,t)=u(1,t),\qquad t\geqslant 0. \tag{7c}$$

The corresponding semi-discretisation is

$$\mathbf{M}_L\frac{\mathrm{d}\mathbf{u}}{\mathrm{d}t}+c\mathbf{M}_R\mathbf{u}=c\mathbf{b}v_0, \tag{8a}$$

$$\mathbf{M}_L^*\frac{\mathrm{d}\mathbf{v}}{\mathrm{d}t}-c\mathbf{M}_R^*\mathbf{v}=c\mathbf{b}^*u_N, \tag{8b}$$

where for positive advection velocity $\mathbf{M}_L$, $\mathbf{M}_R$ and $\mathbf{b}$ are the same as in Eq. (2). $\mathbf{M}_L^*$, $\mathbf{M}_R^*$ and $\mathbf{b}^*$ are obtained from $\mathbf{M}_L$, $\mathbf{M}_R$ and $\mathbf{b}$ by multiplication with the reverse unit matrix (see Appendix A) and $\mathbf{v}=\{v_j\}_{j=0}^{N-1}$. We assume that the corresponding inhomogeneous scalar initial-boundary-value problem, Eq. (2), is stable. Assuming vanishing initial conditions f_u for Eq. (8a), the solution $u_N(s)$ at the grid point $x=x_N$ can be written as

$$u_N(s)=\big[h(s)-u_N(s)(-g_{v_0}(s))\big]g_{u_N}(s), \tag{9}$$

where $g_{u_N}(s)$ and $g_{v_0}(s)$ are the transfer functions of the scalar components between inflow grid point and outflow grid point and $h(s)$ is the homogeneous solution of Eq. (8b) at the outflow grid point ($x=x_0$). Correspondingly, non-vanishing initial conditions of Eq. (8a) are considered by assuming vanishing ones of Eq. (8b). The general case is obtained by superposition. The product $g_{u_N}(s)(-g_{v_0}(s))$ is termed open-loop transfer function. Defining the overall transfer function

$$g_{\mathbf{o}}(s)=\frac{g_{u_N}(s)}{1+g_{u_N}(s)(-g_{v_0}(s))}, \tag{10}$$

Eq. (9) can be expressed as

$$u_N(s)=g_{\mathbf{o}}(s)h(s). \tag{11}$$

A block-diagram representation of the linear feedback system is shown in Fig. 2. Linear-system theory states that the system is stable if and only if the overall transfer function $g_{\mathbf{o}}$ has poles in the left half-plane only [8]. Due to the temporally decaying homogeneous solution of Eq. (2) required for stability, a

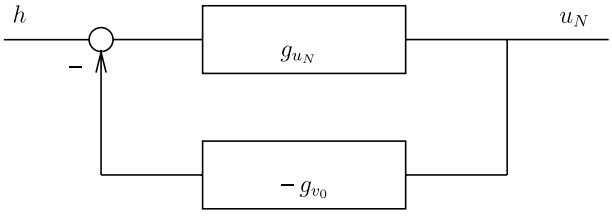

Fig. 2. Feedback system.

temporally decaying excitation $h(s)$ is considered here only. Therefore, $g_{\mathbf{o}}$ may have poles also on the imaginary axis. For stability analysis of the system (i.e., for testing whether the open-loop transfer function becomes unity in the right half-plane) the Nyquist criterion [8] is used.

For open-loop transfer functions with no poles in the right half-plane, the Nyquist criterion states that a feedback system is stable if and only if its open-loop transfer locus does not pass through and does not encircle the point $-1 + \mathrm{i}0$. The open-loop transfer locus is the response of the system along a contour on the imaginary axis from $-\mathrm{i}\infty$ to $+\mathrm{i}\infty$ and back on a half-circle with infinite radius in the right half-plane (Fig. 3, for the transfer locus see e.g. Fig. 4). In the present case of a decaying homogeneous solution, the open-loop transfer function can be allowed to become unity on the imaginary axis so that passes through the point $-1 + \mathrm{i}0$ do not lead to instability. Therefore, a sufficient criterion for stability is given by

$$|g_{u_N}(s)g_{v_0}(s)| \leqslant 1 \quad \text{for } s = \mathrm{i}\Omega \text{ and } |s| \to \infty \text{ with } \delta > 0, \tag{12}$$

which is satisfied for $|g_{u_N}(s)| \leqslant 1$ and $|g_{v_0}(s)| \leqslant 1$, written in compact notation corresponding to Eq. (4)

$$|g_N(s)| \leqslant 1 \quad \text{for } s = \mathrm{i}\Omega \text{ and } |s| \to \infty \text{ with } \delta > 0. \tag{13}$$

For $|s| \to \infty$ the transfer function $g_N(s)$ vanishes on the right half-plane (refer to Eq. (4)). It remains to check whether the amplitude response $g_N(\mathrm{i}\Omega)$, which is symmetric with respect to the origin, is less than or equal to one.

The criterion Eq. (13) is sufficient not only for the single-domain problem considered here but also for multiple domains. In the latter case, the transfer functions $g_{u_N}(s)$ and $g_{v_0}(s)$ are replaced by the product of the single-domain transfer functions, $g_{u_N}(s) = g_{u_{N1}}(s) \cdots g_{u_{Nn}}(s), g_{v_0}(s) = g_{v_{01}}(s) \cdots g_{v_{0n}}(s)$. If the scalar initial-boundary-value problems (Eq. (2)) of all domains are asymptotically stable and in addition satisfy Eq. (13), stability of the multiple-domain composition is guaranteed.

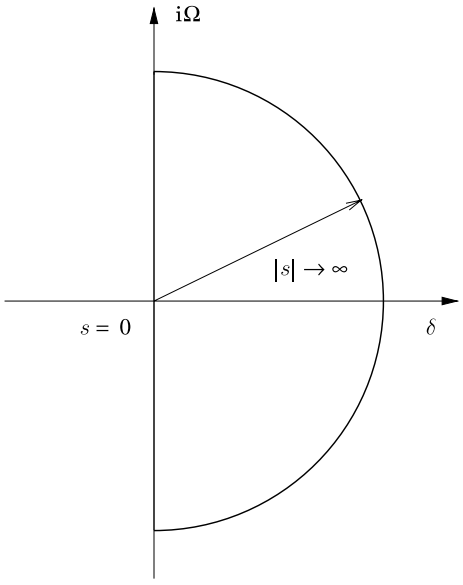

Fig. 3. Contour which encloses the right complex half-plane.

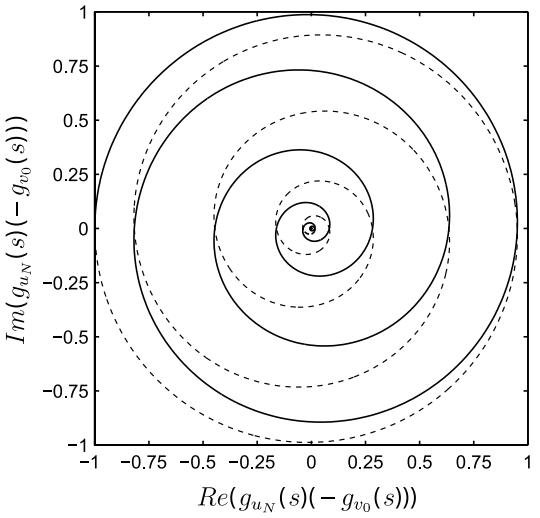

Fig. 4. Nyquist diagram [8] of first-order upwind scheme (UPW1), 2×2 system, $N = 50$: —, $\mathrm{Im}(s) \geqslant 0$; ---, $\mathrm{Im}(s) < 0$.

5. Dispersion properties

Besides stability, dispersion properties of a finite-difference scheme are important. They will also be used for optimisation purposes in the following section. The temporal ansatz $u_n(t) = \hat{u}_n(\Omega)\mathrm{e}^{\mathrm{i}\Omega t}$ applied to the interior scheme of the discretised linear advection Eq. (2)

$$\frac{\partial}{\partial t}\sum_{\mu=-\mu_l}^{\mu_r}\tilde{m}_{L\ n,n+\mu}u_{n+\mu}(t) + \frac{c}{\Delta x}\sum_{\nu=-\nu_l}^{\nu_r}\tilde{m}_{R\ n,n+\nu}u_{n+\nu}(t) = 0 \tag{14}$$

gives

$$\mathrm{i}\Omega\sum_{\mu=-\mu_l}^{\mu_r}\tilde{m}_{L\ n,n+\mu}\hat{u}_{n+\mu}(\Omega) + \frac{c}{\Delta x}\sum_{\nu=-\nu_l}^{\nu_r}\tilde{m}_{R\ n,n+\nu}\hat{u}_{n+\nu}(\Omega) = 0 \tag{15}$$

($\tilde{m}_{L\ n,n+\mu}, \tilde{m}_{R\ n,n+\nu}$ are the interior coefficients of $\tilde{\mathbf{M}}_L, \tilde{\mathbf{M}}_R$, see Appendix A). Assuming spatial wave-like fundamental solutions

$$\hat{u}_{n+1}(\Omega) = \hat{u}_n(\Omega)\kappa \tag{16}$$

with $\kappa = \mathrm{e}^{-\mathrm{i}\xi\Delta x}$ (where ξ is the wavenumber and κ is the space shift operator), one obtains the polynomial

$$\mathrm{i}\Omega\sum_{\mu=-\mu_l}^{\mu_r}\tilde{m}_{L\ n,n+\mu}\kappa^{\mu} + \frac{c}{\Delta x}\sum_{\nu=-\nu_l}^{\nu_r}\tilde{m}_{R\ n,n+\nu}\kappa^{\nu} = 0. \tag{17}$$

Eq. (17) is the dispersion relation of the interior scheme constituting a relation between wavenumber ξ and frequency Ω. Without dissipation the propagation velocity of wave packages is given by the group velocity [21]

$$u_g = \frac{\partial\Omega}{\partial\xi}. \tag{18}$$

This does not necessarily hold for wave propagation with dissipation [4]. Stability of the discretisation implies propagation directions toward non-increasing amplitudes. For the CEN2 scheme the space shift operators are

$$\kappa_{1,2} = -\mathrm{i}\left(\frac{\Omega\Delta x}{c}\right) \pm \sqrt{1 - \left(\frac{\Omega\Delta x}{c}\right)^2} \tag{19}$$

with real wavenumbers $\xi_{1,2}$ if the frequency magnitude $|\Omega|$ is less than or equal to the cutoff frequency, $|\Omega| \leqslant c/\Delta x$, where $\partial\Omega/\partial\xi_1$ and $\partial\Omega/\partial\xi_2$ correspond to positive and negative group velocities respectively, see [21]. When the frequency exceeds the cutoff frequency, the wavenumbers become complex corresponding to exponentially decaying fundamental solutions in space (Fig. 5(a)). For the sixth-order central scheme, as applied in the PAD6 discretisation, there are additional roots with complex wavenumbers (Fig. 5(b)) corresponding to spatially decaying solutions. In contrast to central finite-difference schemes, for which two wavenumbers are real at frequencies below the cutoff frequency, wavenumbers of dissipative schemes become complex in general (for CUVB see Fig. 5(c)). For the first-order upwind scheme there is only one forward-travelling fundamental solution (not displayed). Fig. 6 shows the dispersion properties of CUVB with respect to real wavenumbers, as pertinent to spatial periodicity, resulting in complex fre-

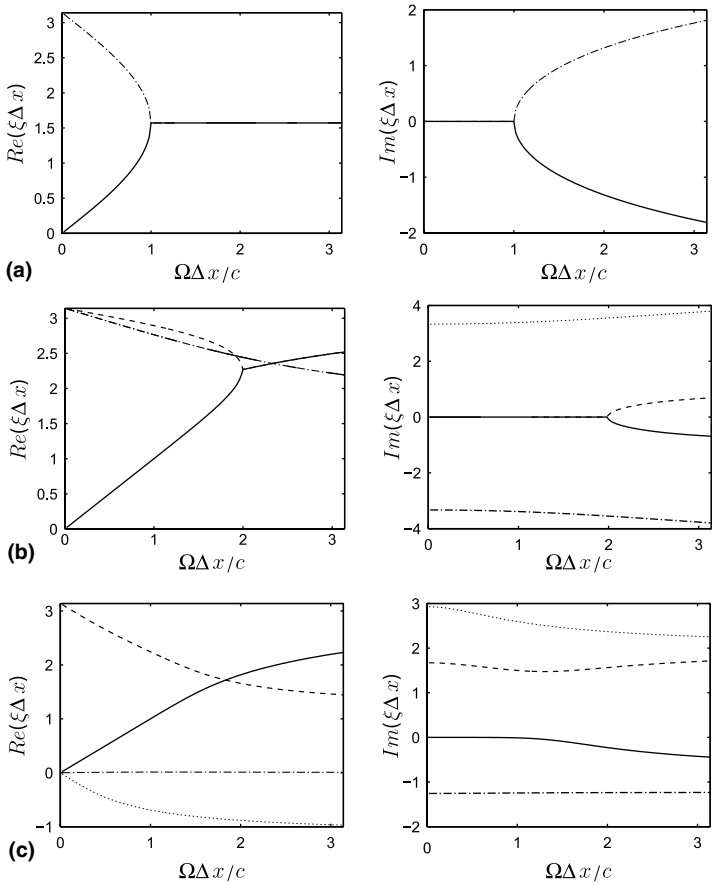

Fig. 5. Dispersion properties of (a) second-order central scheme (CEN2) [21], (b) sixth-order central scheme (PAD6) and (c) scheme CUVB (Ω real, ξ complex): —, regular solution; -·-, ---, ···, spurious solutions.

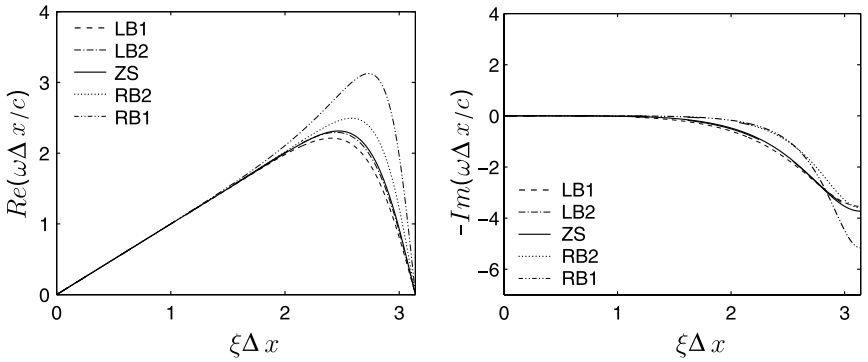

Fig. 6. Dispersion properties of scheme CUVB (ξ real, ω complex) [3].

quencies denoted by ω. In addition to the interior scheme (ZS), the discretisations at the boundaries are evaluated (LB1, LB2, RB2, RB1 represent $n = 1$, 2, $N - 1$ and N in Eq. (17), respectively).

At the inflow and outflow boundary propagating waves are reflected. Reflections occur in general at discontinuities of the discretisation where the coefficients of the scheme change from one grid point to the next. For a quantification of the reflection at the downstream boundary of the CEN2 discretisation see e.g. [20]. Considering the frequency response as a linear combination of the fundamental solutions, Eq. (16), of the interior scheme, components $\mathbf{r}_i$ ($i = 1, \ldots, n$, $n =$ number of fundamental solutions) of the frequency response can be determined according to

$$\begin{bmatrix} r_{k,1}(\mathrm{i}\Omega) \\ r_{k,2}(\mathrm{i}\Omega) \\ \vdots \\ r_{k,n}(\mathrm{i}\Omega) \end{bmatrix} = \begin{bmatrix} \kappa_1^0 & \kappa_2^0 & \ldots & \kappa_n^0 \\ \kappa_1^1 & \kappa_2^1 & \ldots & \kappa_n^1 \\ \vdots & \vdots & & \vdots \\ \kappa_1^{n-1} & \kappa_2^{n-1} & \ldots & \kappa_n^{n-1} \end{bmatrix}^{-1} \begin{bmatrix} g_k(\mathrm{i}\Omega) \\ g_{k+1}(\mathrm{i}\Omega) \\ \vdots \\ g_{k+n-1}(\mathrm{i}\Omega) \end{bmatrix} \quad \text{with } 0 \leqslant k \leqslant N - n + 1. \tag{20}$$

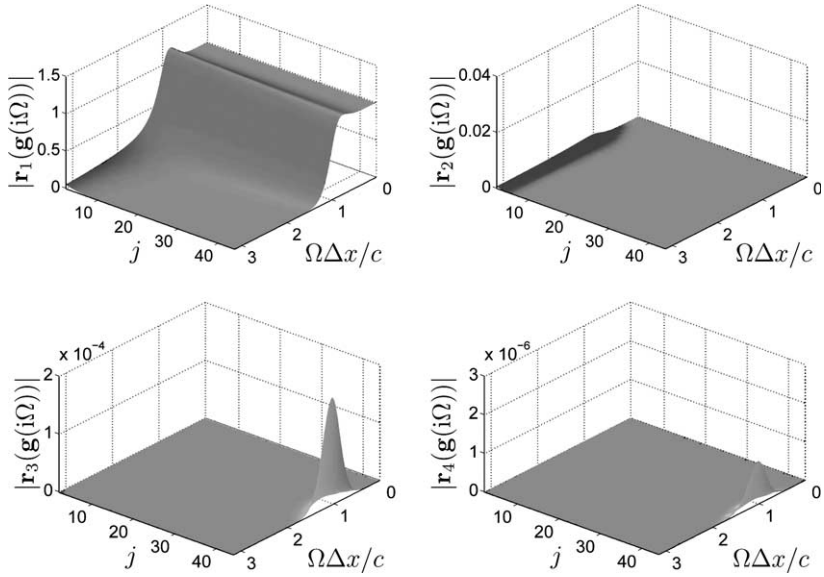

Fig. 7. Magnitude of frequency response decomposed into fundamental solutions $\mathbf{r}_1, \ldots, \mathbf{r}_4$ for scheme CUVB.

Fig. 7 shows the amplitude of the linear components for CUVB where the boundary grid points with discretisation different from the interior one are excluded for clarity. For this dissipative scheme spurious fundamental solutions due to reflections do not spread across the computational domain.

If we consider the frequency response $\mathbf{g}(\mathrm{i}\Omega)$ as a result of superimposed forward and backward travelling waves these waves are consecutively reflected at the boundaries. As mentioned before, significant resonances occur for the central schemes CEN2, PAD6 and SBP6 (Fig. 1).

6. Optimisation procedure

New boundary schemes for the fifth-order compact upwind-biased wavenumber-optimised finite-difference scheme CUVB [2] are now constructed, while the interior scheme is retained. These schemes satisfy the requirement of stability for systems and they are optimised with respect to wave propagation through the boundaries. The original stencil widths and orders of the boundary schemes are maintained, i.e. fifth-order at the points adjacent to the boundary points and fourth-order at the boundary points (for completeness the CUVB coefficients are listed in Appendix B, Eq. (B.1)). A scheme of order r satisfies the order conditions [3]

$$j \sum_{\mu=-\mu_l}^{\mu_r} \mu^{j-1} \tilde{m}_{L\ n,n+\mu} = \sum_{\nu=-\nu_l}^{\nu_r} \nu^j \tilde{m}_{R\ n,n+\nu} \quad \text{for } j = 0, \ldots, r+1. \tag{21}$$

For an approximation of given order there are two free parameters for each boundary scheme. The constraint on these free parameters that all real parts of eigenvalues of Eq. (3) are less than zero,

$$\mathrm{Re}(\lambda) < 0, \tag{22}$$

provides asymptotic stability for the scalar initial-boundary-value problem. Together with the criterion Eq. (13), which in integral formulation gives the constraint

$$\int_0^\infty \max(|g_N(\mathrm{i}\Omega)| - 1, 0)\, \mathrm{d}\Omega = 0, \tag{23}$$

the scheme is stable for systems.

Considering the fact that for the upwind-biased scheme spurious fundamental solutions of Eq. (17) experience larger spatial dissipation than the regular one, it is assumed that spurious waves generated due to reflections at one boundary do not influence the other boundary significantly. The amplitude response at the outflow decreases for an increasing number of grid points due to spatial dissipation of the regular fundamental solution. This implies that for upwind-biased dissipative schemes a minimum number of grid points is required to ensure stability for systems, so that a sufficient amount of dissipation compensates amplifications at the boundaries.

The free parameters are determined by an optimisation with respect to the dispersion properties under the constraints Eqs. (22) and (23) which ensure the desired stability properties. The target of optimisation is to keep the reflections at the boundaries, which generate spurious waves, at a low level and to allow for an undisturbed transmission of waves. A particular point is to obtain amplitude responses close to unity in the low frequency range so that boundary conditions imposed are represented accurately. Reflections and transmission of waves are not quantified as outlined in [19,20]. Rather, we employ the fact that for optimal wave propagation the dispersion relations of the interior scheme and boundary schemes should match. For this purpose, the cost function of the optimisation is chosen similarly as for the optimisation procedure in [3],

$$f_t = \int_0^{1.9} \mathrm{Re}(\omega(\xi)_{LB1} - \omega(\xi)_{ZS})^2 + \mathrm{Re}(\omega(\xi)_{LB2} - \omega(\xi)_{ZS})^2 + \mathrm{Re}(\omega(\xi)_{RB2} - \omega(\xi)_{ZS})^2 + \mathrm{Re}(\omega(\xi)_{RB1} - \omega(\xi)_{ZS})^2 \,\mathrm{d}\xi, \tag{24}$$

considering real wavenumbers only. For wavenumbers larger than the upper bound of integration, dissipation is assumed to be dominant. Furthermore, the requirement of an amplitude response to be close to unity can be enforced approximately for the present problem by the additional constraint

$$\int_0^{\infty} \max(|g_1(\mathrm{i}\Omega)| - 1, 0)\,\mathrm{d}\Omega = 0. \tag{25}$$

This constraint prevents amplifications adjacent to the inflow.

The optimisation is done with a sequential quadratic programming method (SQP) [13] similarly as in [3] using MATLAB [1] for $N = 50$ grid points. The integrals Eqs. (23) and (25) are evaluated numerically for $0 \leqslant \Omega \leqslant \pi c/\Delta x$ using Simpson's rule with 251 grid points. For the integration of Eq. (24) 50 integration points are used. With suitable initial guesses and numerical tolerances of the optimisation, the scheme CUVB-O1 was found, whose coefficients are listed in Appendix B. Note that the optimisation delivers local extrema only and not necessarily a global optimum.

Linear stability is guaranteed by this procedure but does not necessarily hold for the nonlinear case. It does hold for small perturbations from linearity but the stability for eigenvalues on the imaginary axis, representing non-decaying solutions, can be destroyed [12]. Systems considered here (the linear one Eq. (7), for the nonlinear case see next section) do have such eigenvalues if the physical non-decaying solutions are properly represented. In order to obtain stability for nonlinear problems (see next section) it appears reasonable to impose an additional constraint of a maximum amplitude response adjacent to the inflow $\max_{\Omega}(g_1(\mathrm{i}\Omega)) = 1.26$ as an alternative to Eq. (25), where the value 1.26 has been chosen empirically. As result, the scheme CUVB-O2 is obtained (coefficients are given in Appendix B).

The amplitude response of the scheme CUVB-O1 is close to unity at low frequencies and does not exceed this value significantly (Fig. 8). For the scheme CUVB-O2, the amplitude response is larger than unity for intermediate frequencies where the overshoot decays from inflow to outflow (Fig. 8). At the inflow, the overshoot is larger and at a larger frequency than for scheme CUVB (Fig. 1(e)) but decays faster towards the outflow. Fig. 9 shows the dispersion properties of CUVB-O1 and CUVB-O2 evaluated for real wavenumbers. At the lower wavenumber range the properties of the boundary scheme match those of the interior scheme. The split of the amplitude responses into their fundamental solutions according to Eq. (20) shows that for CUVB-O1 the regular waves are not amplified at the inflow (Fig. 10) whereas for

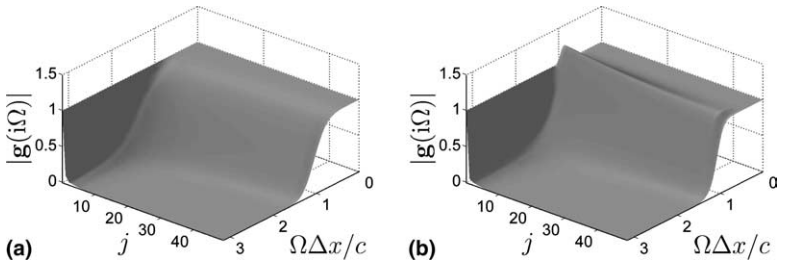

Fig. 8. Amplitude response versus frequency $\Omega\Delta x/c$ along grid points j of fifth-order compact upwind-biased optimised schemes: (a) CUVB-O1 and (b) CUVB-O2.

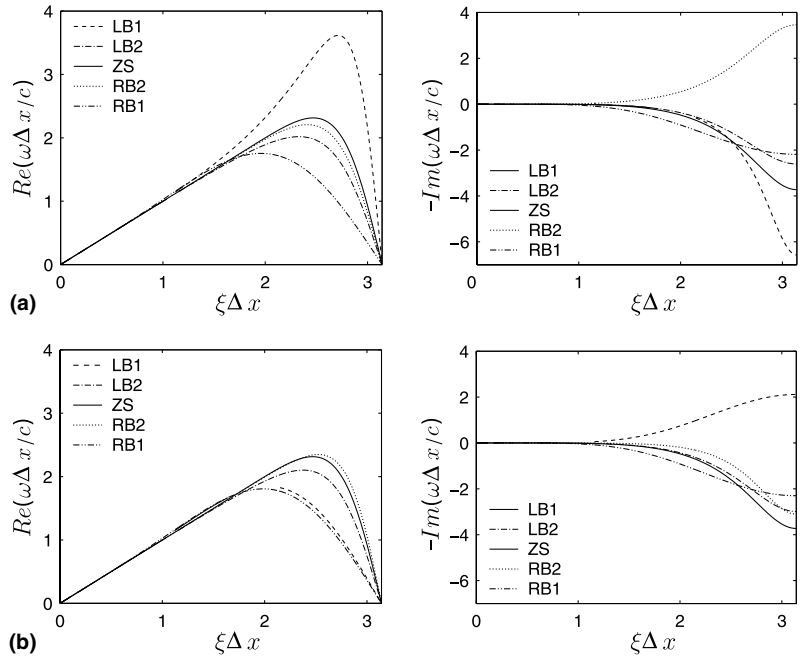

Fig. 9. Dispersion properties of scheme: (a) CUVB-O1 and (b) CUVB-O2.

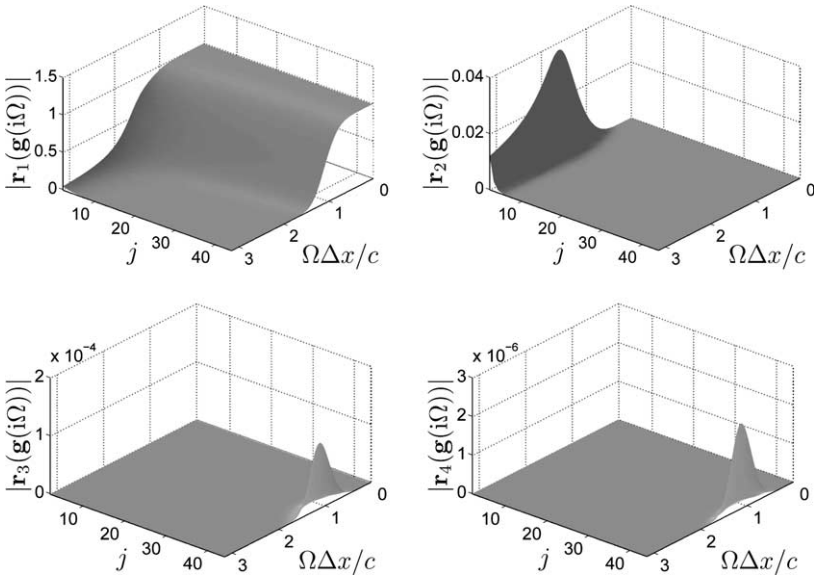

Fig. 10. Magnitude of frequency response decomposed into fundamental solutions $\mathbf{r}_1, \ldots, \mathbf{r}_4$ for scheme CUVB-O1.

CUVB-O2 (Fig. 11) they are amplified. As is the case for scheme CUVB, spurious solutions generated on the boundaries are not significant due to their strong dissipation.

Asymptotic stability of the finite-difference schemes CUVB-O1 and CUVB-O2 for the scalar case and for systems is ensured for $N = 50$ grid points. As mentioned before, for this resolution the constraints for

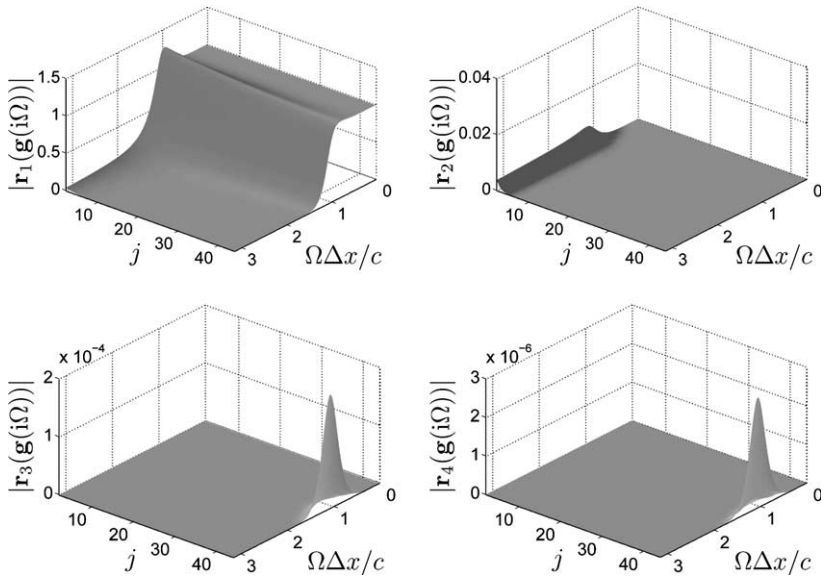

Fig. 11. Magnitude of frequency response decomposed into fundamental solutions $\mathbf{r}_1,\ldots,\mathbf{r}_4$ for scheme CUVB-O2.

stability (Eqs. (22) and (23)) were applied within the optimisation. An investigation of the eigenvalues of the scalar initial-value problem Eq. (3) for different resolutions for schemes CUVB-O1 and CUVB-O2 (and also CUVB) does not exhibit eigenvalues with real parts larger than or equal to zero for resolutions between $N = 10$ to $N = 300$. This is a strong indication for asymptotic stability in the scalar case. The additional stability condition for systems, Eq. (23), is satisfied for resolutions from $N = 10$ to $N = 300$ for CUVB-O1 and from $N = 50$ to $N = 300$ for CUVB-O2, respectively. The original discretisation CUVB [2] shows this stability property for systems for resolutions from $N = 200$ to $N = 300$. Moreover, it confirms the asymptotic stability for systems provided the number of grid points exceeds a certain threshold.

A necessary condition for Lax stability is boundedness of the real parts of eigenvalues which is guaranteed by asymptotic stability [6]. Furthermore, a grid convergence study for the scalar problem and for the 2×2 system has been performed [7], see Table 1. For time integration an eighth-order Runge–Kutta–Fehlberg method [12] with time stepping CFL $= 0.1$ is used so that the temporal truncation error is negligible compared to the spatial error. Time-dependent inflow boundary conditions require a special treatment, for Runge–Kutta schemes, to maintain the full temporal order of accuracy [5]. Here, this is achieved by imposing the inflow boundary condition of the scalar problem at the end of each full

Table 1
Grid convergence at $t = 20$ using initial values $u(x, 0) = \sin(2\pi x)$, $v(x, 0) = -\sin(2\pi x)$

Grid	CUVB-O1				CUVB-O2			
	Scalar case (Eq. (1))		2×2 system (Eq. (7))		Scalar case (Eq. (1))		2×2 system (Eq. (7))	
	$\log L_2$	Rate	$\log L_2$	Rate	$\log L_2$	Rate	$\log L_2$	Rate
51	−6.8295		−5.8834		−6.5754		−4.8806	
101	−8.3451	5.03	−7.4364	5.16	−8.1102	5.10	−6.4031	5.06
151	−9.2282	5.02	−8.3332	5.09	−9.0011	5.06	−7.2897	5.04
201	−9.8537	5.01	−8.9585	5.01	−9.6314	5.04	−7.9189	5.04

Runge–Kutta time-step only [5]. The implied reduced *CFL* number for stability is acceptable for this testing purpose. With this space–time discretisation the L_2 error has been computed at the time $t = 20$. The convergence to the solution, for $\Delta x \to 0$ at a fixed time, implies that the schemes are Lax stable.

7. Applications

The schemes are applied for flow simulations based on the Euler and Navier–Stokes equations. For a one-dimensional configuration, a standing wave between two walls is simulated. The linearisation of the 1D Euler equations for small disturbances between two walls corresponds to the 2×2 system of Eq. (7), where sound waves propagate with the speed of sound. Due to zero velocity of the base flow there is no propagating entropy wave. The upwind discretisation is applied to the conservative formulation of the Euler equations

$$\frac{\partial U}{\partial t} + \nabla \cdot F(U) = 0, \tag{26}$$

where the spatial derivatives of fluxes are discretised with the positive and negative upwind-biased scheme (for notation see Appendix A)

$$\mathbf{D}_i = \frac{1}{\Delta x}(\tilde{\mathbf{M}}_L^{-1}\tilde{\mathbf{M}}_R \otimes \mathbf{F}(\mathbf{U}))_i, \quad \mathbf{D}_i^* = \frac{1}{\Delta x}(\tilde{\mathbf{M}}_L^{*-1}\tilde{\mathbf{M}}_R^* \otimes \mathbf{F}(\mathbf{U}))_i, \tag{27}$$

respectively. Considering the diagonalisation of the flux Jacobian $\Lambda = S(\partial F/\partial U)S^{-1}$, the resulting derivatives of fluxes are determined according to

$$\tilde{\mathbf{D}}_i = \mathbf{S}_i([1 + \operatorname{sgn}(\Lambda_i)]\mathbf{S}_i^{-1}\mathbf{D}_i/2 + [1 - \operatorname{sgn}(\Lambda_i)]\mathbf{S}_i^{-1}\mathbf{D}_i^*/2) \tag{28}$$

(see [3]). Boundary conditions are imposed by setting the velocity normal to the wall to zero. The temporal discretisation is the same as in the linearised case, with a sufficiently small CFL number.

An alternative to the discretisation with boundary schemes, Eq. (27), is to model walls by imposing symmetry conditions (see also Appendix C). Note that in the case of two symmetry conditions the configuration resembles a periodic problem. Corresponding to a periodic initial-value problem with symmetric initial values, stability for the symmetric discretisation is guaranteed by stability of the periodic one (for stability in case of periodic problems see [3]).

We consider a standing wave which has a pressure amplitude of 10^{-5} and a wavenumber equal to unity (pressure, velocity of sound and domain size are scaled to unity). Table 2 shows the maximum L_2 error of pressure within several time intervals $0 < t \leqslant T$ for the scheme CUVB-O2 and the discretisation with symmetry conditions using 50 and 100 grid points. The error growth with time is approximately linear. Applying the scheme CUVB-O1 the error growth becomes exponential (not tabulated), indicating nonlinear

Table 2
L_2 error of pressure for a standing wave within time interval $0 < t \leqslant T$

$\max_{0<t\leqslant T}(L_2)$	CUVB-O2		CUVB/symmetry	
T	$N = 50$	$N = 100$	$N = 50$	$N = 100$
10	4.864050×10^{-10}	4.815339×10^{-10}	4.863170×10^{-10}	4.815313×10^{-10}
50	2.429095×10^{-09}	2.404754×10^{-09}	2.428683×10^{-09}	2.404726×10^{-09}
100	4.856990×10^{-09}	4.808785×10^{-09}	4.856308×10^{-09}	4.808740×10^{-09}
1000	4.846567×10^{-08}	4.807760×10^{-08}	4.848651×10^{-08}	4.807761×10^{-08}

Table 3
Simulation of an inviscid neutral linear-stability eigensolution in plane Couette flow, $c_{\text{lin}} = 1.143770$ for $\alpha = 2$, $M_\infty = 2$ [10]

	$\lvert c_{r,\text{DNS}} - c_{r,\text{lin}}\rvert_{\text{RMS}}$	$\bar{c}_{r,\text{DNS}}$	$\lvert c_{i,\text{DNS}} - c_{i,\text{lin}}\rvert_{\text{RMS}}$	$c_{i,\text{en DNS}}/2$
First time step				
u	1.312×10^{-5}	1.143768	4.008×10^{-7}	-5.024×10^{-7}
w	1.488×10^{-5}	1.143772	8.635×10^{-5}	
p	9.098×10^{-5}	1.143759	1.309×10^{-5}	
T	3.372×10^{-4}	1.143816	2.752×10^{-5}	
T = 1000				
u	6.301×10^{-7}	1.143770	8.896×10^{-7}	-6.000×10^{-7}
w	7.105×10^{-7}	1.143770	6.920×10^{-7}	
p	2.921×10^{-7}	1.143770	1.035×10^{-6}	
T	4.435×10^{-5}	1.143775	5.493×10^{-5}	

instability of this linearly stable scheme. This does not necessarily imply instability for a formulation of the governing equations and discretisation different from Eq. (26)–(28).

As a more complex case, the development of a 2D linear-stability eigensolution of compressible plane Couette flow is simulated using CUVB-O2. The base flow is parallel between an isothermal moving wall and an adiabatic wall at rest as investigated in [10]. The Mach number is $M_\infty = 2$ and the viscosity of the base flow is determined according to Sutherland's law with $Su/T_\infty = 110.4K/220.8K$ for an isothermal wall temperature of $T_W = 1$ (lengths are referred to the wall distance, time to the reference length divided by the velocity of the isothermal wall, pressure to the density times the square of the velocity at this wall and all other variables to their isothermal wall values). Further parameters are a Prandtl number of $Pr = 0.72$ and a ratio of specific heats $\gamma = 1.4$. In the inviscid limit the mode considered $c_{\text{lin}} = 1.143770$ is neutrally stable for $\alpha = 2$, see [10]. The eigensolution has been calculated with a shooting method [10] using the Runge–Kutta scheme as applied for time discretisation and 981 equidistant grid points. For $Re = 10^4$ viscous fluxes are added which are discretised by the PAD6 scheme. While for the inviscid simulation a boundary scheme is used on the upper and lower wall, for the viscous case the lower wall is modelled by symmetry conditions (see Appendix C for the modelling of the wall). The viscous eigensolution ($c_{\text{lin}} = 1.135676 - \text{i} \cdot 8.089441 \times 10^{-3}$) has been determined by a single-domain Chebychev collocation method [15] using 256 Chebychev points.

Table 4
Simulation of a viscous linear-stability eigensolution in plane Couette flow, $c_{\text{lin}} = 1.135676 - \text{i} \cdot 8.089441 \times 10^{-3}$ for $\alpha = 2$, $M_\infty = 2$, $Re = 10^4$

	$\lvert c_{r,\text{DNS}} - c_{r,\text{lin}}\rvert_{\text{RMS}}$	$\bar{c}_{r,\text{DNS}}$	$\lvert c_{i,\text{DNS}} - c_{i,\text{lin}}\rvert_{\text{RMS}}$	$c_{i,\text{en DNS}}/2$
First time step				
u	1.460402×10^{-2}	1.133696	1.081499×10^{-2}	-7.937826×10^{-3}
w	6.306392×10^{-2}	1.141243	6.017972×10^{-2}	
p	2.323833×10^{-2}	1.133223	3.142047×10^{-2}	
T	2.441014×10^{-2}	1.133739	2.493703×10^{-2}	
T = 1000				
u	1.085929×10^{-3}	1.134591	7.898664×10^{-3}	-7.898694×10^{-3}
w	1.081721×10^{-3}	1.134595	7.891802×10^{-3}	
p	1.087211×10^{-3}	1.134589	7.895210×10^{-3}	
T	1.490893×10^{-3}	1.134482	7.898104×10^{-3}	

In Tables 3 and 4 the computed eigensolutions for a disturbance amplitude of $A = 10^{-5}$ (based on the maximum of the streamwise velocity) and a resolution of 50×50 grid points are shown. They are determined for the first time step and for the time interval from $t = 0$ to $t = 1000$ without using intermediate points of the interval. The phase velocity averaged in the wall-normal direction $\bar{c}_{r,\mathrm{DNS}}$ is computed along with its *RMS* error $|c_{r,\mathrm{DNS}} - c_{r,\mathrm{lin}}|_{\mathrm{RMS}}$. Also the RMS error of the scaled growth rate $|c_{i,\mathrm{DNS}} - c_{i,\mathrm{lin}}|_{\mathrm{RMS}}$ and the scaled growth rate based on disturbance energy $c_{i,\mathrm{en\ DNS}}$ are given. As seen, the solution always remained stable and quite accurate.

8. Conclusions

Asymptotic stability of finite-difference discretisations of 2×2 systems has been investigated. These systems correspond to feedback-coupled systems of linear-system theory for which the Nyquist criterion is a necessary and sufficient criterion for asymptotic stability. Stability for systems results if the scheme is stable for the scalar case and, according to the Nyquist criterion, if its amplitude response at the outflow grid point is less than or equal to unity. This requirement covers also the case of multiple domains.

Two new sets of boundary schemes for the fifth-order compact upwind-biased finite-difference scheme CUVB [2] were constructed, referred to as CUVB-O1 and CUVB-O2. They provide stability for systems and were optimised with respect to their dispersion properties. The requirement of asymptotic stability for systems applies to flow cases in which consecutive reflections of sound waves occur, as for a domain surrounded by solid walls. The linearly stable scheme CUVB-O1 satisfies this requirement even for coarse resolutions (as low as ten points, whereas scheme CUVB [2] requires at least 200 points) and has a favorable amplitude response (see Fig. 8(a)). Unfortunately it was found to be potentially unstable for nonlinear problems. However, it is well suited for applications to linear problems such as the linearised Euler equations. The alternative discretisation CUVB-O2 was found to be stable for grids with at least 50 points. It has been tested successfully for the full Euler and Navier–Stokes equations and was thereby found to be stable also in the nonlinear cases investigated. Inviscid and viscous linear-stability eigensolutions of compressible Couette flow were reproduced in good agreement with predictions of linear stability theory.

Acknowledgments

This work was supported by the Swiss National Science Foundation. The authors would like to acknowledge helpful discussions with Prof. J. Waldvogel (ETH), Dr. B. Müller (Uppsala), S. Müller and F. Keiderling.

Appendix A. Discretisation matrices

Considering the finite-difference discretisation

$$\tilde{\mathbf{M}}_L \frac{\mathrm{d}\mathbf{u}}{\mathrm{d}x} = \frac{1}{\Delta x} \tilde{\mathbf{M}}_R \mathbf{u}, \tag{A.1}$$

the matrices of the discretised initial-boundary-value problem Eq. (2) using a strong (i.e.direct, non-approximate) imposition of the inflow boundary condition are given by

$$m_{L\ k,l} = \tilde{m}_{L\ k+1,l+1} - \tilde{m}_{L\ 1,l+1} \frac{\tilde{m}_{L\ 1,1}}{\tilde{m}_{L\ k+1,1}}, \tag{A.2a}$$

$$m_{R\ k,l} = \frac{1}{\Delta x}\left(\tilde{m}_{R\ k+1,l+1} - \tilde{m}_{R\ 1,l+1}\frac{\tilde{m}_{L\ 1,1}}{\tilde{m}_{L\ k+1,1}}\right), \tag{A.2b}$$

$$b_k = \frac{1}{\Delta x}\left(\tilde{m}_{R\ k+1,1} - \tilde{m}_{R\ 1,1}\frac{\tilde{m}_{L\ 1,1}}{\tilde{m}_{L\ k+1,1}}\right). \tag{A.2c}$$

The matrices for negative advection velocity, Eq. (8b), are

$$\begin{aligned} \mathbf{M}_L^* &= \mathbf{P}\mathbf{M}_L\mathbf{P} \\ \mathbf{M}_R^* &= -\mathbf{P}\mathbf{M}_R\mathbf{P} \quad \text{with } \mathbf{P} = \begin{bmatrix} 0 & & 1 \\ & \iddots & \\ 1 & & 0 \end{bmatrix}, \\ \mathbf{b}^* &= \mathbf{P}\mathbf{b} \end{aligned} \tag{A.3}$$

the reverse unit matrix.

Note that the spatial operators $\tilde{\mathbf{M}}_L$ and $\tilde{\mathbf{M}}_R$ are asymptotically stable and Lax stable, also for systems, by satisfying the summation-by-parts condition [7]. To maintain stability if the boundary conditions are imposed, the penalty formulation SAT [7] can be used, as done for determining the amplitude response of the SBP6 scheme, Fig. 1(d). The matrices of the semi-discretisation of Eq. (2) are determined with a penalty parameter $\tau = 2$ [7].

Appendix B. Upwind-biased schemes

For the compact upwind-biased finite-difference scheme CUVB [2] the discretisation matrices are

$$\tilde{\mathbf{M}}_L = \begin{bmatrix} 1 & 1.344856712172 & -1.655143287828 & & & & 0 \\ -1.384173201496 & 1 & 6.620636755258 & -2.122934969145 & & & \\ -0.152087544263 & 0.2375084218594 & 1 & -0.104175088526 & 0.018754210929673 & & \\ & \ddots & \ddots & \ddots & \ddots & \ddots & \\ & -0.152087544263 & 0.2375084218594 & 1 & -0.104175088526 & 0.018754210929673 & \\ & & 15.74839515424 & 27.04931646417 & 1 & -0.3211206221354 & \\ 0 & & & 4.850969558221 & 7.826957363797 & 1 & \end{bmatrix}, \tag{B.1a}$$

$$\tilde{\mathbf{M}}_R = \begin{bmatrix} -2.557476118695 & 3.982714931742 & -0.9827149317416 & -0.4425238813046 & 0 & 0 \\ 3.362325146817 & -11.84525146073 & 8.836922058206 & 0.2990810938894 & -0.6530768381839 & \\ 0.354175088526 & -1.550033687437 & 1.025050531156 & 0.1832996458959 & -0.012491578140655 & \\ & \ddots & \ddots & \ddots & \ddots & \ddots \\ & 0.354175088526 & -1.550033687437 & 1.025050531156 & 0.1832996458959 & -0.012491578140655 \\ & -1.846602572079 & -30.2283794418 & 21.15923086495 & 12.27649588754 & -1.36074473861 \\ 0 & 0.0020010162019952 & -0.6538343569155 & -8.740436045696 & 5.756444175312 & 3.635825211098 \end{bmatrix}. \tag{B.1b}$$

They provide an order of accuracy of five at the interior points and at the points adjacent to the boundary points, and an order of four at the boundary points.

The boundary schemes of CUVB were optimised with respect to reflection and transmission of waves, as explained in Section 6, using Eq. (24) as cost function and the constraints Eqs. (22), (23) and (25), with $\tilde{m}_{L\ 1,2}, \tilde{m}_{L\ 1,3}, \tilde{m}_{L\ 2,3}, \tilde{m}_{L\ 2,4}, \tilde{m}_{L\ N-1,N-2}, \tilde{m}_{L\ N-1,N-3}, \tilde{m}_{L\ N,N-1}$ and $\tilde{m}_{L\ N,N-2}$ being the variables for the

optimisation within a range of $[-100, 100]$. For $N = 50$ and suitable initial guesses we obtain the following scheme CUVB-O1,

$$\tilde{\mathbf{M}}_L = \begin{bmatrix} 1 & -1.96378909730 & -5.38218806239 & & & 0 \\ -0.922162677719 & 1 & 6.72212514508 & -0.207233947492 & & \\ -0.152087544263 & 0.2375084218594 & 1 & -0.104175088526 & 0.018754210929673 & \\ & \ddots & \ddots & \ddots & \ddots & \ddots \\ & -0.152087544263 & 0.2375084218594 & 1 & -0.104175088526 & 0.018754210929673 \\ & & -28.7262198889 & 73.3089889001 & 1 & -19.1497197889 \\ 0 & & & -13.7434120690 & 80.3037792329 & 1 \end{bmatrix}, \tag{B.2a}$$

$$\tilde{\mathbf{M}}_R = \begin{bmatrix} -2.04090173087 & 9.22461628934 & -5.94568364596 & -1.27289749294 & 0.0348665804236 & 0 \\ 2.24861883630 & -9.10701778134 & 4.57733895440 & 2.57917157018 & -0.298111579533 & \\ 0.354175088526 & -1.550033687437 & 1.025050531156 & 0.1832996458959 & -0.012491578140655 & \\ & \ddots & \ddots & \ddots & \ddots & \ddots \\ & 0.354175088526 & -1.550033687437 & 1.025050531156 & 0.1832996458959 & -0.012491578140655 \\ & 8.41987410001 & 1.09881702593 & -102.038489200 & 140.667981700 & -48.1481836260 \\ 0 & -7.58726594183 & 47.9808309958 & -117.4556688493 & 53.7575413147 & 23.3045624806 \end{bmatrix}. \tag{B.2b}$$

An alternative optimisation with the constraint Eq. (25) replaced by $\max_{\Omega}(g_1(\mathrm{i}\Omega)) = 1.26$ results in the scheme CUVB-O2,

$$\tilde{\mathbf{M}}_L = \begin{bmatrix} 1 & 14.8137755383 & 0.172558101067 & & & 0 \\ -1.08391180127 & 1 & 6.76200737753 & -0.827642286727 & & \\ -0.152087544263 & 0.2375084218594 & 1 & -0.104175088526 & 0.018754210929673 & \\ & \ddots & \ddots & \ddots & \ddots & \ddots \\ & -0.152087544263 & 0.2375084218594 & 1 & -0.104175088526 & 0.018754210929673 \\ & & 3.85733435009 & 7.30522519306 & 1 & -0.00320394465427 \\ 0 & & & -9.33790001714 & 81.6392242488 & 1 \end{bmatrix}, \tag{B.3a}$$

$$\tilde{\mathbf{M}}_R = \begin{bmatrix} -5.77239737614 & -8.45985168260 & 19.2206633074 & -5.95851570175 & 0.970101453100 & 0 \\ 2.64062039134 & -10.0908066001 & 5.99319883390 & 1.87308727772 & -0.416099902825 & \\ 0.354175088526 & -1.550033687437 & 1.025050531156 & 0.1832996458959 & -0.012491578140655 & \\ & \ddots & \ddots & \ddots & \ddots & \ddots \\ & 0.354175088526 & -1.550033687437 & 1.025050531156 & 0.1832996458959 & -0.012491578140655 \\ & -0.439699140931 & -7.58032349424 & 4.27638969117 & 3.78763206561 & -0.0439991216105 \\ 0 & -7.33142702216 & 45.7115454692 & -119.458836373 & 57.8074201959 & 23.2712977303 \end{bmatrix}. \tag{B.3b}$$

Appendix C. Adiabatic wall

In this contribution, isothermal walls are taken into account by strong imposition of the velocities and temperatures on the boundary grid points. Adiabatic walls are modelled by symmetry of the density and energy and antisymmetry of the velocities with respect to the wall. By this means the boundary conditions of zero velocity (wall at rest) and zero heat flux are satisfied. The resulting zero pressure gradient normal to the wall $\nabla p \cdot \mathbf{n} = 0$, is an acceptable approximation for high Reynolds number flow. For explicit schemes, this corresponds to the use of ghost points outside the domain for which the values are set according to this conditions. In our case the symmetry and antisymmetry conditions are implicitly imposed by the discretisation using the coefficients of the interior scheme only,

$$
\begin{aligned}
l_1 &:= \tilde{m}_{L\ n,n-2}, \quad l_2 := \tilde{m}_{L\ n,n-1}, \quad l_3 := \tilde{m}_{L\ n,n}, \quad l_4 := \tilde{m}_{L\ n,n+1}, \quad l_5 := \tilde{m}_{L\ n,n+1}, \\
r_1 &:= \tilde{m}_{R\ n,n-2}, \quad r_2 := \tilde{m}_{R\ n,n-1}, \quad r_3 := \tilde{m}_{R\ n,n}, \quad r_4 := \tilde{m}_{R\ n,n+1}, \quad r_5 := \tilde{m}_{R\ n,n+1}.
\end{aligned} \tag{C.1}
$$

For upwind-biased schemes, there is a coupled discretisation for positive and negative advection velocity. Modelling adiabatic walls on opposed boundaries of the domain, the symmetric (upper signs) and antisymmetric (lower signs) case is discretised by

$$
\tilde{\mathbf{M}}_{LS} \begin{bmatrix} \mathbf{d} \\ \mathbf{d}^* \end{bmatrix} = \tilde{\mathbf{M}}_{RS} \mathbf{u} \tag{C.2}
$$

with

$$
\tilde{\mathbf{M}}_{LS} = \begin{bmatrix}
l_3 & l_4 & l_5 & & & & 0 & 0 & 0 & \mp l_2 & \mp l_1 & & & & & 0 \\
l_2 & l_3 & l_4 & l_5 & & & & 0 & 0 & \mp l_1 & & & & & & \\
l_1 & l_2 & l_3 & l_4 & l_5 & & & 0 & 0 & & & & & & & \\
 & \ddots & & \ddots & & \ddots & \ddots & \ddots & \vdots & \vdots & & & & & & \\
 & & l_1 & l_2 & l_3 & l_4 & l_5 & 0 & 0 & & & & & & & \\
 & & & l_1 & l_2 & l_3 & l_4 & 0 & 0 & & & & & & & \mp l_5 \\
0 & & & & l_1 & l_2 & l_3 & 0 & 0 & & & & & & \mp l_5 & \mp l_4 \\
\pm 1 & 0 & \cdots & & & \cdots & 0 & 0 & 1 & 0 & \cdots & & & \cdots & 0 & 0 \\
0 & 0 & \cdots & & & \cdots & 0 & 1 & 0 & 0 & \cdots & & & \cdots & 0 & \pm 1 \\
\mp l_4 & \mp l_5 & & & & & & 0 & 0 & l_3 & l_2 & l_1 & & & & 0 \\
\mp l_5 & & & & & & & 0 & 0 & l_4 & l_3 & l_3 & l_1 & & & \\
 & & & & & & & 0 & 0 & l_5 & l_4 & l_3 & l_2 & l_1 & & \\
 & & & & & & & \vdots & \vdots & & \ddots & \ddots & \ddots & \ddots & \ddots & \\
 & & & & & & & 0 & 0 & & l_5 & l_4 & l_3 & l_2 & l_1 & \\
 & & & & & & \mp l_1 & 0 & 0 & & & l_5 & l_4 & l_3 & l_2 & \\
0 & & & & & \mp l_1 & \mp l_2 & 0 & 0 & 0 & & & l_5 & l_4 & l_3 &
\end{bmatrix}, \tag{C.3a}
$$

$$
\tilde{\mathbf{M}}_{RS} = \begin{bmatrix}
r_3 & r_4 \pm r_2 & r_5 \pm r_1 & & & & & & 0 \\
r_2 & r_3 \pm r_1 & r_4 & r_5 & & & & & \\
r_1 & r_2 & r_3 & r_4 & & r_5 & & & \\
 & \ddots & & \ddots & \ddots & & \ddots & & \\
 & & r_1 & r_2 & r_3 & & r_4 & r_5 & \\
0 & & & r_1 & r_2 & & r_3 \pm r_5 & r_4 & \\
0 & \cdots & & & & & \cdots & 0 & \\
0 & \cdots & & & & & \cdots & 0 & \\
-r_4 & -(r_3 \pm r_5) & -r_2 & -r_1 & & & & 0 & \\
-r_5 & -r_4 & -r_3 & -r_2 & & -r_1 & & & \\
 & \ddots & & \ddots & \ddots & & \ddots & & \\
 & & -r_5 & & -r_4 & -r_3 & -r_2 & -r_1 & \\
 & & & & -r_5 & -r_4 & -(r_3 \pm r_1) & -r_2 & \\
0 & & & & & -(r_5 \pm r_1) & -(r_4 \pm r_2) & -r_3 &
\end{bmatrix}. \tag{C.3b}
$$

References

[1] MATLAB 6.5 User's Guide, The Math Works, Inc., Natick, MA, 2002.

[2] N.A. Adams, Direct numerical simulation of turbulent compression ramp flow, Theoretical and Computational Fluid Dynamics 12 (1998) 109–129.

[3] N.A. Adams, K. Shariff, A high-resolution hybrid compact-ENO scheme for shock-turbulence interaction problems, Journal of Computational Physics 127 (1996) 27–51.
[4] L. Brillouin, Wave Propagation in Periodic Structures, second ed., Dover Publications, New York, 1953.
[5] M. Carpenter, D. Gottlieb, S. Abarbanel, W.-S. Don, The theoretical accuracy of Runge–Kutta time discretizations for the initial boundary value problem: a study of the boundary error, SIAM Journal on Scientific Computing 16 (6) (1995) 1241–1252.
[6] M.H. Carpenter, D. Gottlieb, S. Abarbanel, The stability of numerical boundary treatments for compact high-order finite-difference schemes, Journal of Computational Physics 108 (1993) 272–295.
[7] M.H. Carpenter, D. Gottlieb, S. Abarbanel, Time-stable boundary conditions for finite-difference schemes solving hyperbolic systems: methodology and application to high-order compact schemes, Journal of Computational Physics 111 (1994) 220–236.
[8] D.K. Cheng, Analysis of Linear Systems, Addison-Wesley Publishing Company, Reading, MA, 1959.
[9] T. Colonius, Modeling artificial boundary conditions for compressible flow, Annual Review of Fluid Mechanics 36 (2004) 315–345.
[10] P.W. Duck, G. Erlebacher, M.Y. Hussaini, On the linear stability of compressible plane Couette flow, Journal of Fluid Mechanics 258 (1994) 131–165.
[11] B. Gustafsson, The convergence rate for difference approximations to mixed initial boundary value problems, Mathematics of Computation 29 (130) (1975) 396–406.
[12] E. Hairer, S.P. Nørsett, G. Wanner, Solving Ordinary Differential Equations I, second ed., Springer, Berlin, 1993.
[13] W. Hock, K. Schittkowski, A comparative performance evaluation of 27 nonlinear programming codes, Computing 30 (1983) 335–358.
[14] S.K. Lele, Compact finite difference schemes with spectral-like resolution, Journal of Computational Physics 103 (1992) 16–42.
[15] M.R. Malik, Numerical methods for hypersonic boundary layer stability, Journal of Computational Physics 86 (1990) 376–413.
[16] B. Strand, Numerical studies of hyperbolic IBVP with high-order finite difference operators satisfying a summation by parts rule, Applied Numerical Mathematics 26 (1998) 497–521.
[17] A.I. Tolstykh, M.V. Lipavskii, On performance of methods with third- and fifth-order compact upwind differencing, Journal of Computational Physics 140 (1998) 205–232.
[18] L.N. Trefethen, Group velocity interpretation of the stability theory of Gustafsson, Kreiss, and Sundström, Journal of Computational Physics 49 (1983) 199–217.
[19] L.N. Trefethen, Stability of finite-difference models containing two boundaries or interfaces, Mathematics of Computation 45 (172) (1985) 279–300.
[20] R. Vichnevetsky, Wave propagation analysis of difference schemes for hyperbolic equations: a review, International Journal for Numerical Methods in Fluids 7 (1987) 409–452.
[21] R. Vichnevetsky, J.B. Bowles, Fourier Analysis of Numerical Approximations of Hyperbolic Equations, SIAM, Philadelphia, 1982.